6th European Conference on Computational Mechanics (ECCM 6)
7th European Conference on Computational Fluid Dynamics (ECFD 7)
11 - 15 June 2018, Glasgow, UK

NUMERICAL INVESTIGATION OF SPLIT FORM NODAL DISCONTINUOUS GALERKIN SCHEMES FOR IMPLICIT LES OF A TURBULENT CHANNEL FLOW

Michael Bergmann[1*], Rebecca Gölden[1] and Christian Morsbach[1]

[1] German Aerospace Center (DLR),
Institute of Propulsion Technology,
Linder Höhe, 51147 Cologne, Germany
Michael.Bergmann@dlr.de, Rebecca.Goelden@dlr.de, Christian.Morsbach@dlr.de

Key words: Discontinuous Galerkin, Spectral Element Method, LES, Channel flow

Abstract. Gassner et al. *(Split form nodal discontinuous Galerkin schemes with summation - by - parts property for the compressible Euler equations. Journal of Computational Physics, 327:3966, Dec. 2016)* proposed a promising alternative stabilization technique for the discontinuous Galerkin scheme, which relies on the reformulation of the non-linear advection terms into split forms. It has been observed, that these split forms can stabilize the inviscid Taylor Green Vortex with high-order approximations, which are unstable with over-integration.

In this paper, we apply different split form discontinous Galerkin schemes for the implicit large eddy simulation of a fully developed turbulent channel flow and investigate their robustness and accuracy for wall-bounded flows. Furthermore, we compare these results to implicit large eddy simulation with over-integrated high-order approximations in terms of statistical values and turbulence spectra. Finally, we show that the use of high-order split form discontinuous Galerkin scheme can significantly improve the results in comparison to low-order discretizations.

1 INTRODUCTION

Through the increasingly severe requirements on emission and noise pollution of modern turbomachinery, there is a high demand for new and more efficient engine technologies. To further progress the improvements of such technologies, more precise numerical methods are required in order to accurately investigate turbomachinery flows. With the known predictive deficiencies of unsteady Reynolds averaged Navier-Stokes (URANS) simulations, which are currently the state-of-the-art simulation methodology in the design process of turbomachinery, and the increasing computational ressources, scale-resolving simulations, e.g. large eddy simulations (LES), are becoming more popular methods to further study the unsteady phenomena of complex flows [1]. Due to efficiency advantages for highly accurate simulations and favorable dissipation/dispersion properties, high-order spatial

discretizations, such as the discontinuous Galerkin (DG) method, are attractive numerical methods for LES. Precisely, the dissipation errors of the DG method only have an impact on higher wavenumber, leaving low and medium frequencies unaffected, cf. [2, 3]. This inherent property of the DG scheme leads to a dissipation of the smallest scales. Therefore, a common LES approach within the DG community is to perform an implicit LES (iLES), where no explicit subgrid-scale model is used and the dissipation is entirely realized by the numerical discretization scheme, [4, 5].

As it turns out, the stabilization provided from the upwind dissipation typically used in DG schemes is insufficient for under-resolved turbulent flows. Especially, high polynomial approximation orders with their lower inherent dissipation are often unstable without an additional stabilization mechanism. However, it can be noted that it is possible to achieve reasonably accurate results for under-resolved turbulent flows with high-order DG approximations when a proper stabilization technique is applied [6].

One of the most popular stabilization strategies in the DG community is polynomial de-aliasing, often also denoted as over-integration [7]. The mechanism focusses directly on the source of the numerical instabilities, the under-integration of the non-linear advective flux terms, by increasing the number of integration nodes according to the non-linearity. Nevertheless, when we apply the DG ansatz on the conserved quantities, the advective flux functions of the Navier-Stokes equations cannot be integrated exactly with standard quadrature rules because they are rational polynomials of the conserved quantities. As a consequence, Moura et al. show in [3] that even high-order DG discretizations with the number of quadrature nodes increased by a factor of four in each spatial direction are unstable for the under-resolved simulation of the inviscid Taylor-Green-Vortex.

Recently, a very promising stabilization technique for the nodal DG scheme has been proposed by Gassner et al., which is in fact able to stabilize the inviscid Taylor-Green-Vortex [8]. It is based on the diagonal-norm summation-by-parts (SBP) property of the discontinuous Galerkin spectral element method (DGSEM) with Legendre-Gauss-Lobatto (LGL) nodes and relies on the reformulation of the advective flux terms into an average of the conservative and advective forms. In [9], it is shown for a frozen burgers turbulence scenario that through using an average of the conservative form, which overestimates the energy at higher wavenumbers, and the advective form, which underestimates the energy at higher wavenumbers, the aliasing errors are balanced. The authors believe that this mechanism helps improve the robustness in under-resolved simulations by keeping the growth of the energy under a certain level. Furthermore, in the same article, the accuracy of a split form DG scheme has been compared to an over-integrated DG discretization for the inviscid Taylor-Green-Vortex. Both stabilization techniques showed similar results for moderate high-orders (around sixth order).

In this paper, we apply different split form DG schemes for an iLES of a fully developed turbulent channel flow and investigate their robustness and accuracy. Additionally, we compare these results to simulations with over-integrated DG schemes in terms of statistical quantities and turbulence spectra. All investigated schemes are integrated into DLR's in-house solver for turbomachinery flows TRACE, which is developed at DLR's Institute of Propulsion Technology.

2 NUMERICAL METHODS

2.1 Governing equations

Three-dimensional compressible flow is described by the Navier-Stokes equations, which can be expressed in conservation form as

$$\frac{\partial \boldsymbol{q}}{\partial t} + \nabla_x \cdot \boldsymbol{F}(\boldsymbol{q}, \nabla_x \boldsymbol{q}) = 0, \tag{1}$$

with suitable initial and boundary conditions. Here, $\boldsymbol{q}$ denotes the conservative state vector $\boldsymbol{q} = (\rho, \rho u_1, \rho u_2, \rho u_3, \rho E)^T$ with $\boldsymbol{u} = (u_1, u_2, u_3)$ and ∇_x is the gradient operator in physical space. The physical flux $\boldsymbol{F}$ is equal to the difference of advective and viscous fluxes, $\boldsymbol{F} = \boldsymbol{F}^a(\boldsymbol{q}) - \boldsymbol{F}^v(\boldsymbol{q}, \nabla_x \boldsymbol{q})$, which are defined as follows

$$\boldsymbol{F}_l^a = \begin{pmatrix} \rho u_l \\ \rho u_1 u_l + \delta_{1l} p \\ \rho u_2 u_l + \delta_{2l} p \\ \rho u_3 u_l + \delta_{3l} p \\ \rho H u_l \end{pmatrix}, \quad \boldsymbol{F}_l^v = \begin{pmatrix} 0 \\ \tau_{1l} \\ \tau_{2l} \\ \tau_{3l} \\ \tau_{lj} v_j - q_l \end{pmatrix}, \tag{2}$$

where $l = 1, 2, 3$ are the Cartesian components of the physical flux $\boldsymbol{F} = (\boldsymbol{F}_1, \boldsymbol{F}_2, \boldsymbol{F}_3)$. The pressure p is related to the other thermodynamic variables by the equation of state for an ideal gas, which is $p = (\gamma - 1)\rho\,[E - 1/2(\boldsymbol{u} \cdot \boldsymbol{u})]$, where $\gamma = 1.4$ is the ratio between the specific heats of the fluids. The total enthalpy H is equal to $H = E + p/\rho$.

2.2 Discontinuous Galerkin discretization

This work focusses on a special case of the DG method, namely the DGSEM, which is based on a collocation of integration and interpolation nodes. With the use of LGL points as nodes, the resulting DGSEM operator has the SBP property, which is the fundamental key for deriving the split form nodal DG scheme, [10, 8].

The domain is subdivided into shape-regular meshes $\mathcal{T}_h = \{K\}$ consisting of non-overlapping elements K, where h denotes a piecewise constant mesh function. For each element $K \in \mathcal{T}_h$, we define a polynomial continuous invertible mapping M^K to a reference element K_{ref} with $\boldsymbol{x} = M^K(\boldsymbol{\xi})$, where $\boldsymbol{x} = (x, y, z)$ are the Cartesian coordinates and $\boldsymbol{\xi} = (\xi, \eta, \zeta)$ are the generalized coordinates of the reference element K_{ref}, cf. [11, 12]. The mapping is used to transform (1) from the physical space into the reference space, which results in

$$J \boldsymbol{q}_t + \nabla_\xi \cdot \boldsymbol{\mathcal{F}}(\boldsymbol{q}, \nabla_x \boldsymbol{q}) = 0, \tag{3}$$

where J is the Jacobian determinant $J(\boldsymbol{\xi}) = \det\left(\frac{\partial \boldsymbol{x}}{\partial \boldsymbol{\xi}}\right)$ and $\boldsymbol{\mathcal{F}}$ is the contravariant flux. The metric terms are constructed following [13] to ensure the free-stream preserving property. For brevity, we restrict this presentation to Cartesian meshes as they are used in our computations. The extension to general curvilinear grids can be found in [8].

Thereafter, the solution vector $\boldsymbol{q}$ is approximated as piecewise polynomial functions and can be expressed by the polynomial expansion

$$\boldsymbol{q}_h(\boldsymbol{\xi},t)|_K = \sum_{n=0}^{N^3} \boldsymbol{q}_n(t)\ \phi_n^N(\boldsymbol{\xi}) \quad \forall K \in \mathcal{T}_h, \tag{4}$$

where the 3D polynomial basis function $\phi_n^N = l_i^N(\xi) l_j^N(\eta) l_k^N(\zeta)$ is constructed in a tensor product fashion with 1D Lagrange polynomials l_i^N of degree N. Following that we multiply (3) by a sufficiently smooth test function $\boldsymbol{v}$, use the same ansatz for the test function $\boldsymbol{v}$ as for the solution (4), integrate by parts and test only against the basis function ϕ_m^N for all $m = 0 \dots N^3$. This yields in

$$\int_{K_{\text{ref}}} J\,(\boldsymbol{q}_h)_t\,\phi_m^N d\boldsymbol{\xi} + \int_{\partial K_{\text{ref}}} \phi_m^N\,(\boldsymbol{\mathcal{H}}^a - \boldsymbol{\mathcal{H}}^v)\,d\boldsymbol{S} - \int_{K_{\text{ref}}} \boldsymbol{\mathcal{F}}(\boldsymbol{q}_h, \nabla_x \boldsymbol{q}_h) \cdot \nabla_\xi \phi_m^N d\boldsymbol{\xi} = 0. \tag{5}$$

Here, $\boldsymbol{\mathcal{H}}^a$ and $\boldsymbol{\mathcal{H}}^v$ denote the surface normal numerical flux function for the advective and viscous terms, respectively. In this work, we apply the local Lax-Friedrichs or Roe's approximative Riemann solver for the advective part, cf. [14]. Furthermore, the discretization of the viscous terms is based on the Bassi and Rebay 2 (BR2) method [15]. The scheme provides an additional artificial dissipation term depending on the jump of the solution at the element interfaces, which can be controlled by a penalty constant η_{BR}. The constant is set to $\eta_{BR} = 6$ for all cases shown.

As stated above, we apply a nodal collocation approach, where we use LGL nodes as integration and interpolation points, cf. [16]. This choice gives rise to an highly efficient scheme as many numerical operations can be omitted, [17]. For example, the 1D mass matrix gets lumped in the following form

$$\boldsymbol{M} = \text{diag}[\omega_0, \dots, \omega_N], \tag{6}$$

where $\{\omega_i\}_{i=0}^N$ are the LGL quadrature weights. In contrast to the above advantages, due to limited precision of the integration and the non-linearity of the advective flux, the scheme is less accurate and can be unstable for under-resolved simulations [6]. A straightforward approach to address this problem is to increase the number of integration points, which is known as over-integrated DGSEM. We follow the procedure described in [6], where the overall polynomial degree M is increased according to the desired number of integration points. The approximate solution is then filtered by a modal cut-off filter before every Runge-Kutta stage to retain only the original number of degrees of freedom (DOF), i.e. $(N+1)^3$ in each element. However, the key of this work is the split form DGSEM, which will be derived in the following.

2.3 Split form DG scheme

The scheme is based on the splitting of the advective flux terms. Thus, we separate the advective contributions $\widetilde{\boldsymbol{\mathcal{F}}}^a = \left(\widetilde{\boldsymbol{\mathcal{F}}}_1^a, \widetilde{\boldsymbol{\mathcal{F}}}_2^a, \widetilde{\boldsymbol{\mathcal{F}}}_3^a\right)$ and the viscous contributions $\widetilde{\boldsymbol{\mathcal{F}}}^{\boldsymbol{v}}$ of (5),

resulting in

$$\int_{K_{\mathrm{ref}}} J\left(\boldsymbol{q}_h\right)_t \phi_m d\boldsymbol{\xi} + \overbrace{\left[\int_{\partial K_{\mathrm{ref}}} \phi_m \boldsymbol{\mathcal{H}}^a d\boldsymbol{S} - \int_{K_{\mathrm{ref}}} \boldsymbol{\mathcal{F}}^a(\boldsymbol{q}) \cdot \nabla_\xi \phi_m d\boldsymbol{\xi}\right]}^{\widetilde{\boldsymbol{\mathcal{F}}}^a} \tag{7}$$
$$\underbrace{-\left[\int_{\partial K_{\mathrm{ref}}} \phi_m \boldsymbol{\mathcal{H}}^v d\boldsymbol{S} - \int_{K_{\mathrm{ref}}} \boldsymbol{\mathcal{F}}^v(\boldsymbol{q}, \nabla_x \boldsymbol{q}) \cdot \nabla_\xi \phi_m d\boldsymbol{\xi}\right]}_{\widetilde{\boldsymbol{\mathcal{F}}}^v} = 0.$$

The advective contributions of each nodal coefficients (i, j, k) in ξ-direction can be rewritten in a strong form, i.e. performing another integration-by-parts, as

$$\left(\widetilde{\boldsymbol{\mathcal{F}}}_1^a\right)_{ijk} = \frac{1}{\boldsymbol{M}_{ii}} \left[\delta_{iN}(\boldsymbol{\mathcal{H}}^a - \boldsymbol{\mathcal{F}}_1^a)_{Njk} - \delta_{i0}(\boldsymbol{\mathcal{H}}^a - \boldsymbol{\mathcal{F}}_1^a)_{0jk}\right] + \sum_{n=0}^{N} \boldsymbol{D}_{in} \left(\boldsymbol{\mathcal{F}}_1^a\right)_{njk}. \tag{8}$$

The remaining directions follow analogously, [16, 8]. Here, $\boldsymbol{D}$ is the 1D polynomial derivative matrix,

$$\boldsymbol{D}_{ij} = \frac{\partial l_j(\xi_i)}{\partial \xi}, \quad i, j = 0, \ldots, N, \tag{9}$$

where $\{\xi_i\}_{i=0}^N$ are the LGL nodes. As mentioned before, the derivative operator $\boldsymbol{D}$ of the LGL approximation satisfies the diagonal-norm SBP property. Based on this property, Fischer et al. [18] and Carpenter et al. [10] constructed an entropy-conservative form of the volume terms by applying a two-point entropy conserving numerical volume flux $\boldsymbol{\mathcal{F}}_1^{a,\#}\left(\boldsymbol{q}_{ijk}, \boldsymbol{q}_{mjk}\right)$. Thus, (8) can be rewritten in an entropy conservative/stable form given by

$$\left(\widetilde{\boldsymbol{\mathcal{F}}}_1^a\right)_{ijk} = \frac{1}{\boldsymbol{M}_{ii}} \left[\delta_{iN}(\boldsymbol{\mathcal{H}}^a - \boldsymbol{\mathcal{F}}_1^a)_{Njk} - \delta_{i0}(\boldsymbol{\mathcal{H}}^a - \boldsymbol{\mathcal{F}}_1^a)_{0jk}\right] + 2\sum_{n=0}^{N} \boldsymbol{D}_{in} \boldsymbol{\mathcal{F}}_1^{a,\#}\left(\boldsymbol{q}_{ijk}, \boldsymbol{q}_{njk}\right). \tag{10}$$

Gassner et al. showed that it is possible to use any symmetric and consistent two-point numerical volume flux and each choice results in a novel variant of DGSEM [8]. Furthermore, the authors identified choices of the numerical volume flux resulting in well known split forms. In this work, we apply the split forms of Ducros [19] and Kennedy and Gruber [20], which can be written as a numerical volume flux [8]

$$\boldsymbol{\mathcal{F}}_{1,\mathrm{Ducros}}^{a,\#}\left(\boldsymbol{q}_{ijk}, \boldsymbol{q}_{njk}\right) = \begin{pmatrix} \{\{\rho\}\}\{\{u_1\}\} \\ \{\{\rho u_1\}\}\{\{u_1\}\} + \{\{p\}\} \\ \{\{\rho u_2\}\}\{\{u_1\}\} \\ \{\{\rho u_3\}\}\{\{u_1\}\} \\ (\{\{\rho E\}\} + \{\{p\}\})\{\{u_1\}\} \end{pmatrix}, \tag{11}$$

$$\boldsymbol{\mathcal{F}}^{a,\#}_{1,\text{KennedyGruber}}\left(\boldsymbol{q}_{ijk},\boldsymbol{q}_{njk}\right)=\begin{pmatrix}\{\{\rho\}\}\{\{u_1\}\}\\ \{\{\rho\}\}\{\{u_1\}\}\{\{u_1\}\}+\{\{p\}\}\\ \{\{\rho\}\}\{\{u_1\}\}\{\{u_2\}\}\\ \{\{\rho\}\}\{\{u_1\}\}\{\{u_3\}\}\\ \{\{\rho\}\}\{\{u_1\}\}\{\{E\}\}+\{\{p\}\}\{\{u_1\}\}\end{pmatrix}. \tag{12}$$

Here, $\{\{\cdot\}\}$ is the spatial average of a quantity, i.e. $\{\{a\}\} := \frac{1}{2}(a_{ijk}+a_{njk})$. Regarding the numerical surface flux function, we replace the central flux with the specific split form flux, but keep the upwind dissipation term of the applied Riemann solver, i.e. Lax-Friedrichs or Roe. Finally, we employ an explicit third-order accurate Runge-Kutta time-stepping method with a constant time step to advance in time.

3 IMPLICIT LES OF A TURBULENT CHANNEL FLOW

In this work, we investigate the numerical schemes for the iLES of a fully developed turbulent channel flow. A computational domain of $2\pi\delta \times 2\delta \times \pi\delta$ is chosen with periodic boundary conditions in stream- (x) and spanwise (z) direction, whereby δ is half of the channel height. A constant body force source term in the streamwise momentum equation is used to enforce the Reynolds number $Re_\tau = \delta u_\tau/\nu = 395$ based on the friction velocity u_τ. A Mach number of $Ma = 0.1$ is chosen to be comparable to the incompressible DNS results of *Iwamoto et al.* [21]. All simulations are performed on a fairly coarse grid with $64 \times 64 \times 64$ DOF with a grid stretching in the wall-normal direction. The resulting effective grid spacing, which is defined as $hu_\tau/\nu/(N+1)$, for different polynomial orders N is given as $\Delta x^{+,N=3,7,15} \approx 39$, $\Delta z^{+,N=3,7,15} \approx 20$, $\Delta y^{+,N=3}_{\text{min}} \approx 1.3$, $\Delta y^{+,N=7}_{\text{min}} \approx 2.0$, $\Delta y^{+,N=15}_{\text{min}} \approx 3.85$. Furthermore, the flow field is initialized with a superposition of a RANS solution and synthetic generated turbulent velocity fluctuations computed following [22]. In order to reach a converged state, a transient phase of 20 eddy turnover times (ETT $= tu_\tau/\delta$) is simulated. Following that, the flow quantities are averaged over another 20 ETT.

Firstly, we consider a polynomial approximation order of $N = 7$, resulting in a mesh of $8 \times 8 \times 8$ elements. If not stated otherwise, Roe's Riemann solver is used in the simulation. Remark that simulations with high-order DGSEM scheme for the test case and this mesh resolution become unstable if no stabilization technique is applied [23]. In Figure 1, the normalized mean streamwise velocity profile U^+ and the root-mean-square (RMS) of the velocity fluctuations are shown over the normalized wall coordinate y^+ for the KennedyGruber scheme, Ducros scheme and the over-integrated DGSEM with $M+1 = 12$ integration points. M denotes the polynomial order of the over-integrated simulation as described in Section 2.2. Despite the coarse resolution, all applied stabilization mechanisms yield in stable and accurate results compared to the DNS data. Moreover, the profiles obtained with KennedyGruber and Ducros scheme are nearly perfectly equal. Comparing the split form results and the over-integrated DGSEM results, one can observe that the over-integrated scheme predicts the streamwise velocity fluctuations more accurately, especially in the buffer layer. On the contrary, the mean velocity profiles of the split forms are closer to the DNS data. This is most likely to an over-prediction of

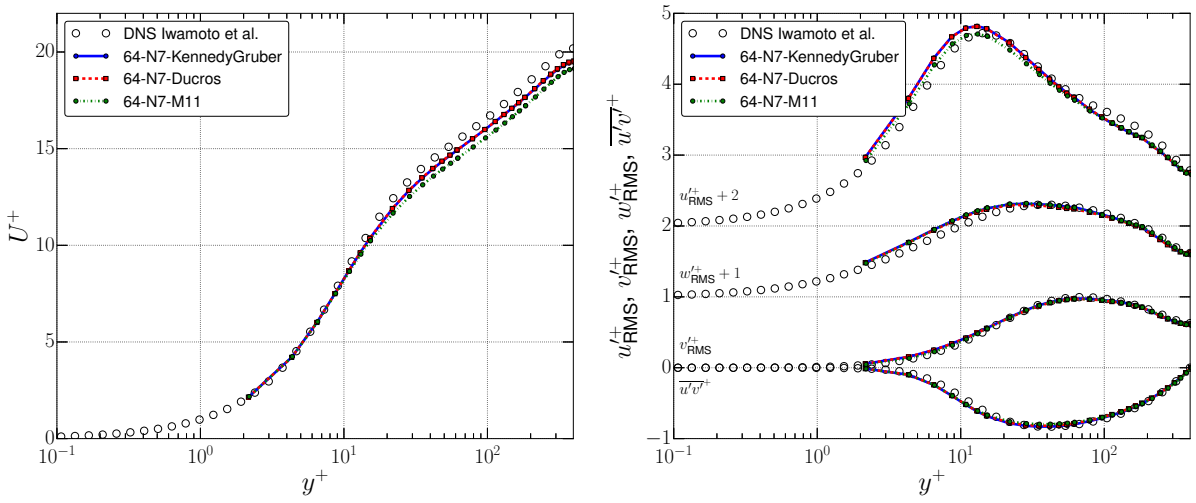

Figure 1: ILES of a turbulent channel flow at $Re_\tau = 395$. Mean streamwise velocity profiles U^+ *(left)* and RMS turbulent velocities u'^+_{RMS}, v'^+_{RMS}, w'^+_{RMS} and shear stresses $\overline{u'v'}$ *(right)* of DGSEM with Kennedy Gruber split form (*blue solid with circles*), DGSEM with Ducros split form (*red dashed with squares*) and over-integrated DGSEM with an over-integration order of $M = 11$ (*green dash dotted with circles*).

the streamwise velocity fluctuations, which results in an increase of the mean velocity. However, especially in the outer layer of the streamwise components, discrepancies to the DNS data are visible for all shown computations, i.e. u'^+_{rms} around $y^+ \approx 130$.

To further analyze the stabilization methods, the one-dimensional energy spectrum in the streamwise direction over the wavenumber k is shown in Figure 2. In order to obtain the spectrum, we probed the quantities over time at equally distanced points along multiple lines in the streamwise direction at $y^+ = 390$. The number of points was equal to the number of DOF in each direction, i.e. $[(N+1) \cdot n_{\mathrm{Element}}]$ and we applied a cell-centered distribution inside of each element, which is $x_i = (i - 1/2)h/(N+1)$, to avoid probing at element interfaces. Hereinafter, we merged all 1D probes of the specific channel height, i.e. $y^+ = 390$, computed the two-point correlations and performed a discrete Fourier transformation of the two-point correlation. Following that, the spectra are plotted up to the theoretical Nyquist frequency. Remark that the resolution of polynomials is theoretically limited to π points per wavelength (PPW), which results in a cut-off wavenumber of $k_c \approx 20.4$ for 64 DOF.

The energy spectra, shown in Figure 2, exhibit a strong drop off of energy in the inertial range, which is a typical behavior for upwind based iLES discretization with a Roe's Riemann solver [24]. Additionally, the cut-off wavenumber $k^{1d}_{1\%}$ according to the 1% rule is plotted, after which the numerical dissipation of the DG scheme becomes relevant, cf. [2, 3]. Despite the fact that the 1% rule was derived for inviscid test cases while this test case features a finite Reynolds number with additional molecular viscosity, $k^{1d}_{1\%}$ is in quite good accordance with the observed energy drop off. Furthermore, it is interesting to note that the obtained spectra are almost equal for all stabilization techniques considered. The numerical dissipation starts within the same points in the inertial range for all schemes. The similarity of the energy spectra of split form DGSEM

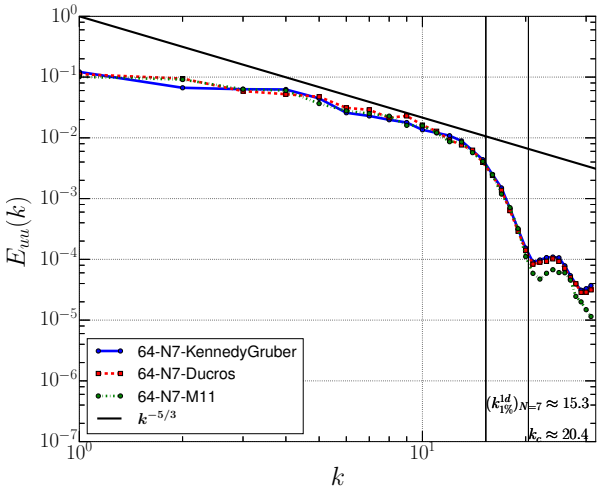

Figure 2: ILES of a turbulent channel flow at $Re_\tau = 395$. One-dimensional energy spectra in the streamwise direction of the streamwise velocity E_{uu} at $y^+ = 390$ obtained with DGSEM with Kennedy-Gruber split form (*blue solid with circles*), DGSEM with Ducros split form (*red dashed with squares*) and over-integrated DGSEM with an over-integration order of $M = 11$ (*green dash dotted with circles*).

and over-integration was also observed in [9] for the inviscid Taylor-Green-Vortex. The same behavior of the schemes is also visible in the energy spectra near to the wall (not shown). The only minor discrepancies between the stabilization techniques emerge after the cut-off wavenumber k_c, where the energy bump of the split forms is slightly higher than the one of the over-integrated DGSEM. As a next investigation, the results for variable approximation orders on the same mesh with $64 \times 64 \times 64$ DOF are displayed in Figure 3. It is remarkable that even the very high-order approximation ($N = 15$) is stable for this considered under-resolution. The standard Legendre-Gauss (LG)-DGSEM is shown here, because it is the highest stable approximation order on this resolution without any stabilization technique applied, cf. [23]. Anyway, a clear trend in the solution quality with increasing order is visible. The low-order version of KennedyGruber DGSEM and standard LG-DGSEM over-predict the streamwise velocity fluctuations by a big amount. On the contrary, the very high-order DGSEM with $N = 15$ under-predicts the peak of the streamwise velocity fluctuations and shows larger discrepancies in the buffer layer than the 8th order DGSEM. Also differences to the DNS data can be observed in spanwise Reynold stresses. One reason for this could be the insufficient wall resolution due to the use of linear elements as y^+_{min} rises with increasing polynomial order. This could be improved by adjustments of the inner element stretching, e.g. use of high-order geometry approximation. Nevertheless, the $N = 15$ results are closest to the DNS data in the outer layer. Looking at the energy spectrum in Figure 3, we see a clear improvement of the numerical dissipation of the scheme as the range of affected wavenumbers is decreased with increasing polynomial order. The start of the influence of the numerical dissipation is in good accordance with the proposed one-dimensional cut-off wavenumber of the 1%-rule $k^{1d}_{1\%}$. Additionally, one can observe that the magnitude of the peak after k_c decreases with increasing polynomial orders.

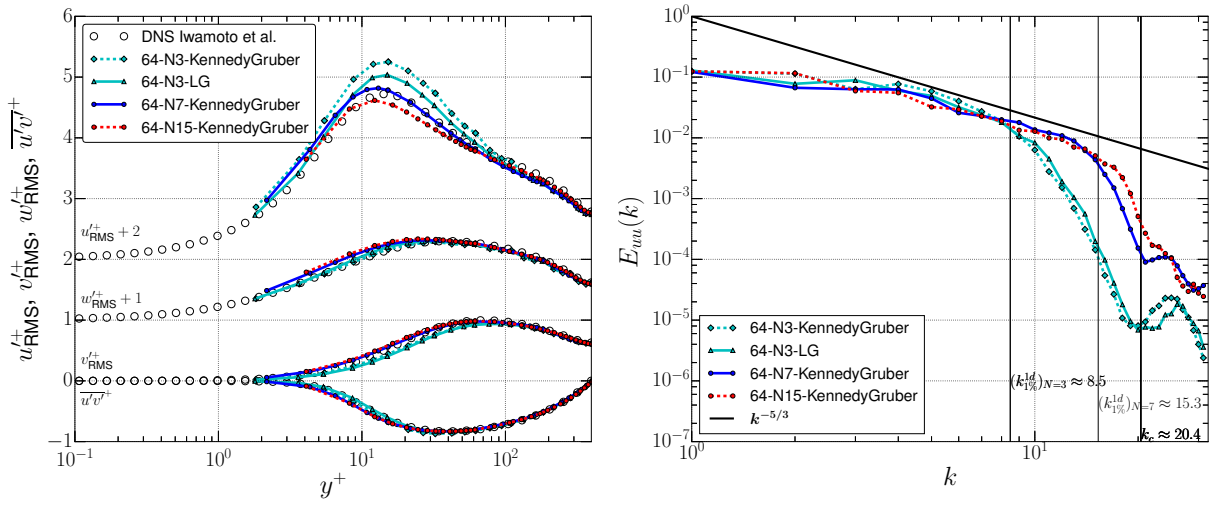

Figure 3: ILES of a turbulent channel flow at $Re_\tau = 395$. RMS turbulent velocities u'^+_{RMS}, v'^+_{RMS}, w'^+_{RMS} and shear stress $\overline{u'v'}$ *(left)* and one-dimensional energy spectra in the streamwise direction of the streamwise velocity E_{uu} *(right)* at $y^+ = 390$ obtained with DGSEM with KennedyGruber split form and $N = 3$ (*cyan dashed with diamonds*), $N = 7$ (*blue solid with circles*), $N = 15$ (*red dashed with circles*) and LG-DGSEM $N = 3$ without stabilization (*cyan solid with triangles*).

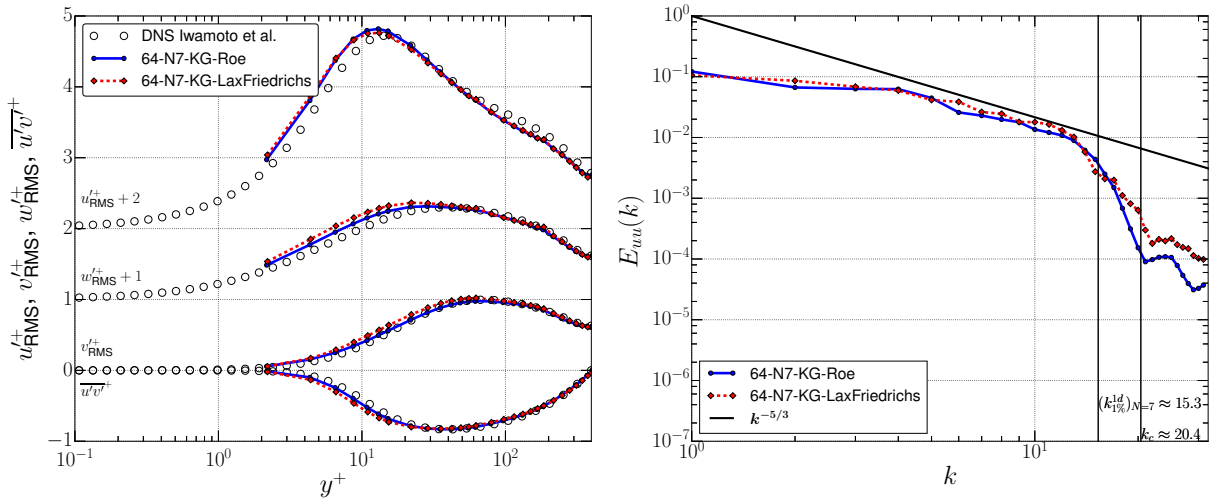

Figure 4: ILES of a turbulent channel flow at $Re_\tau = 395$. RMS turbulent velocities u'^+_{RMS}, v'^+_{RMS}, w'^+_{RMS} and shear stress $\overline{u'v'}$ *(left)* and one-dimensional energy spectra in the streamwise direction of the streamwise velocity E_{uu} *(right)* at $y^+ = 390$ of DGSEM with Roe's (*blue solid with circles*) and with Lax-Friedrichs (LLF) dissipation term (*red dashed with diamonds*).

Finally, we consider the results obtained with KennedyGruber (KG) split form and different Riemann solvers, namely Roe and local Lax-Friedrichs, see Figure 4. Especially in the streamwise and spanwise turbulent velocity fluctuations, larger differences compared to the DNS results can be obtained for the Lax-Friedrichs solver. Aside from that, the wavenumber at which the streamwise energy drops sharply is fairly identical for both Riemann solvers. However, the magnitude of the drop-off is different. Higher energy at

the cut-off wavenumber are present for the Lax-Friedrichs solver. Similar trends are also shown in [3], in which the authors stated that the observed 'energy bump' for schemes with Lax-Friedrichs solver emerges due to the sharper dissipation behavior in wavenumber space.

4 CONCLUSION

In this work, we applied two split form DG schemes, namely Ducros and KennedyGruber, for the implicit LES of a turbulent channel flow with a Reynolds number of $Re_\tau = 395$. On the coarse mesh resolution, the standard DGSEM with LGL nodes crashes with an approximation order greater than $N > 2$. Both split forms are able to stabilize the simulation with a high order approximation. Moreover, the statistical quantities obtained with both split form DG schemes are in good accordance with the DNS results considering the coarse mesh resolution. Comparing the results with the over-integrated DGSEM, one can observe slight advantages of the over-integrated DGSEM due to the higher precision of integration. The obtained one-dimensional energy spectra for both stabilization strategies are nearly identical up to the cut-off wavenumber. Furthermore, we showed that one can improve the results when increasing the approximation order of the split form DG scheme. Especially the range of unaffected wavenumbers is increased when using a high order approximation. However, the use of linear elements without inner element stretching in combination with a very high approximation order, i.e. $N = 15$ probably results in an insufficient near-wall resolution.

We plan to extend the investigation of stabilization strategies to more complex test cases with higher Reynolds numbers. Here, one key observation is the performance of the split forms on curvilinear grids, i.e. curved elements, where geometric aliasing errors occur. Furthermore, compressible effects should also be considered in the upcoming studies. Beyond that, a novel LES approach by *Flad and Gassner* [24], where an energy-preserving split form DG scheme without additional interface dissipation is combined with an explicit subgrid-scale model, shows significant advantages over iLES results and could be a promising strategy for future LES of more complex cases.

REFERENCES

[1] James Tyacke, Paul Tucker, Richard Jefferson-Loveday, Nagabushana Rao Vadlamani, Robert Watson, Iftekhar Naqavi, and Xiaoyu Yang. Large eddy simulation for turbines: Methodologies, cost and future outlooks. *Journal of Turbomachinery*, 136(6):061009–061009–13, November 2013.

[2] R.C. Moura, S.J. Sherwin, and J. Peiró. Linear dispersion-diffusion analysis and its application to under-resolved turbulence simulations using discontinuous Galerkin spectral/hp methods. *Journal of Computational Physics*, 298(C):695–710, October 2015.

[3] R.C. Moura, G. Mengaldo, J. Peiró, and S.J. Sherwin. On the eddy-resolving capability of high-order discontinuous Galerkin approaches to implicit les / under-resolved

dns of euler turbulence. *Journal of Computational Physics*, 330(C):615–623, February 2017.

[4] Andrea D. Beck, Thomas Bolemann, David Flad, Hannes Frank, Gregor J. Gassner, Florian Hindenlang, and Claus-Dieter Munz. High-order discontinuous Galerkin spectral element methods for transitional and turbulent flow simulations. *International Journal for Numerical Methods in Fluids*, 76(8):522–548, August 2014.

[5] C. Carton Wiart, K. Hillewaert, L. Bricteux, and G. Winckelmans. Implicit les of free and wall-bounded turbulent flows based on the discontinuous Galerkin/symmetric interior penalty method. *International Journal for Numerical Methods in Fluids*, 78(6):335–354, March 2015.

[6] Gregor J. Gassner and Andrea D. Beck. On the accuracy of high-order discretizations for underresolved turbulence simulations. *Theoretical and Computational Fluid Dynamics*, 27(3):221–237, 2013.

[7] Robert M. Kirby and George Em Karniadakis. De-aliasing on non-uniform grids: algorithms and applications. *Journal of Computational Physics*, 191(1):249 – 264, 2003.

[8] G. J. Gassner, A. R. Winters, and D. A. Kopriva. Split form nodal discontinuous Galerkin schemes with summation-by-parts property for the compressible euler equations. *Journal of Computational Physics*, 327:39–66, December 2016.

[9] Andrew R. Winters, R.Rodrigo C. Moura, Gianmarco Mengaldo, Gregor J. Gassner, Stefanie Walch, Joaquim Peiró, and Spencer J. Sherwin. A comparative study on polynomial dealiasing and split form discontinuous Galerkin schemes for underresolved turbulence computations. *arXiv preprint, arXiv:1711.10180*, November 2017.

[10] Mark H. Carpenter, Travis C. Fisher, Eric J. Nielsen, and Steven H. Frankel. Entropy stable spectral collocation schemes for the navier–stokes equations: Discontinuous interfaces. *SIAM Journal on Scientific Computing*, 36(5):B835–B867, 2014.

[11] F. Bassi and S. Rebay. High-order accurate discontinuous finite element solution of the 2d Euler equations. *Journal of Computational Physics*, 138(2):251 – 285, 1997.

[12] Svetlana Drapkina, Graham Ashcroft, and Christian Frey. On the integration of high-order boundary eelement in a 3d discontinuous Galerkin method for turbomachinery flows. In *Proceedings Seventh European Congress on Computational Methods in Applied Sciences and Engineering*, Barcelona, Spain, June 2014.

[13] David A. Kopriva. Metric identities and the discontinuous spectral element method on curvilinear meshes. *Journal of Scientific Computing*, 26(3):301, Mar 2006.

[14] E.F. Toro. *Riemann Solvers and Numerical Methods for Fluid Dynamics: A Practical Introduction*. Springer Berlin Heidelberg, 2009.

[15] F. Bassi and S. Rebay. *A High Order Discontinuous Galerkin Method for Compressible Turbulent Flows*, pages 77–88. Springer Berlin Heidelberg, Berlin, Heidelberg, 2000.

[16] David A. Kopriva. *Implementing Spectral Methods for Partial Differential Equations: Algorithms for Scientists and Engineers*. Springer Publishing Company, Incorporated, 1st edition, 2009.

[17] Michael Bergmann, Svetlana Drapkina, Graham Ashcroft, and Christian Frey. A comparison of various nodal discontinuous Galerkin methods for the 3d Euler equations. In *Proceedings Eighth European Congress on Computational Methods in Applied Sciences and Engineering*, Crete, Greek, June 2016.

[18] Travis C. Fisher, Mark H. Carpenter, Jan Nordstrm, Nail K. Yamaleev, and Charles Swanson. Discretely conservative finite-difference formulations for nonlinear conservation laws in split form: Theory and boundary conditions. *Journal of Computational Physics*, 234:353 – 375, 2013.

[19] F. Ducros, F. Laporte, T. Soulres, V. Guinot, P. Moinat, and B. Caruelle. High-order fluxes for conservative skew-symmetric-like schemes in structured meshes: Application to compressible flows. *Journal of Computational Physics*, 161(1):114 – 139, 2000.

[20] Christopher A. Kennedy and Andrea Gruber. Reduced aliasing formulations of the convective terms within the navier-stokes equations for a compressible fluid. *J. Comput. Phys.*, 227(3):1676–1700, January 2008.

[21] K. Iwamoto, Y. Suzuki, and N. Kasagi. Database of fully developed channel flow. Technical report, HTLAB Internal Report No ILR-0201, 2002.

[22] Michael L. Shur, Philippe R. Spalart, Michael K. Strelets, and Andrey K. Travin. Synthetic turbulence generators for rans-les interfaces in zonal simulations of aerodynamic and aeroacoustic problems. *Flow, Turbulence and Combustion*, 93(1):63–92, 2014.

[23] Michael Bergmann, Christian Morsbach, and Martin Franke. Implicit les of a turbulent channel flow with high-order discontinuous Galerkin and finite volume discretization. In *Proceedings ERCOFTAC Direct and Large Eddy Simulations XI*, Pisa, Italy, May 2017.

[24] David Flad and Gregor Gassner. On the use of kinetic energy preserving dg-schemes for large eddy simulation. *Journal of Computational Physics*, 350:782 – 795, December 2017.